Single crystal magnets

N. Ikuta

Miyagi Technical College, Natori, Japan 981-12

M. Okada and M. Homma

Department of Materials Science, Faculty of Engineering, Tohoku University, Sendai, Japan 980

T. Minowa

Shin-Etsu Chemical Industry Company, Takefu, Fukui, Japan 915

Single crystals of the Fe–Cr–Co alloys without and with 3% Mo were prepared by a recrystallization process. The microstructures and the magnetic properties of $\langle 100 \rangle$, $\langle 110 \rangle$, and $\langle 111 \rangle$ single crystals were investigated after the heat treatment in the ridge region of the miscibility gap. The magnetic properties of the Fe–22 Cr–17 Co ridge single crystals were not affected very much by the crystal orientation. However, the Fe–23 Cr–20 Co–3 Mo alloys show the crystal orientation dependence of the magnetic properties. The single crystal alloys are aged in a magnetic field, the direction of which is varied around $\langle 100 \rangle$ axes. The magnetic properties are measured parallel to the applied field directions and are summarized in view of deviated angle from a $\langle 100 \rangle$ axis. The greater the deviation of the applied field direction from a $\langle 100 \rangle$ axis, the poorer are the magnetic properties of the Mo single crystal alloy. The best magnetic properties are achieved with Fe–22 Cr–18.5 Co–3 Mo $\langle 100 \rangle$ ridge single crystal as $Br = 1.58$ T (15.8 kG), $bHc = 72.8$ kA/m (910 Oe), and (BH)max $= 91.2$ kJ/m^3 (11.4 MGOe), which is the highest energy product reported for the Fe–Cr–Co magnet family.

PACS numbers: 81.540.Ef, 81.40.Rs, 75.30. − m, 61.50.Jr

INTRODUCTION

Fe–Cr–Co alloys are potential permanent magnets because of their good ductility and excellent magnetic properties.[1–10] The magnetic hardening of the alloys is performed by heat treating within the miscibility gap, producing modulated structures consisting of two phases, an iron-rich phase (α_1) and a chromium-rich phase (α_2).[11–13]

Recently, Minowa, Okada, and Homma experimentally identified the existence of the ridge of the miscibility gap in an Fe–Cr–Co system suggested by Nishizawa et al.[14] which is the part of the protrusion of the miscibilty gap.[15–17] It was also reported that the magnetic properties of the polycrystalline Fe–Cr–Co alloys were remarkably improved by heat treating within the ridge region of the miscibility gap. An Fe–22 Cr–15 Co alloy achieves the magnetic properties as $Br = 1.56$ T, $bHc = 51.6$ kA/m, and (BH)max $= 66.4$ kJ/m^3 (8.3 MGOe). The improvements of the magnetic properties of the ridge alloys were believed to be due to the highly elongated and aligned FeCo rich particles parallel to the applied magnetic field direction in the Cr rich phase, independently of grain crystal orientations.[17] However, this had not been confirmed so far in using the single crystal alloys. Another reported approach to improve the magnetic properties was to add the Mo to the alloys, which makes the anisotropic decomposition along $\langle 100 \rangle$ directions[18] and utilize the anisotropic decomposition to more efficiently elongate and align the FeCo rich phase in the applied field direction in a $\langle 100 \rangle$ texture sample. This was done with the Fe–24 Cr–15 Co–3 Mo alloy in developing the $\langle 100 \rangle$ columnar structure, which gave the magnetic properties as $Br = 1.54$ T, $bHc = 67.2$ kA/m, and (BH)max $= 76$ kJ/m^3 (Ref. 10). But, the columnar grain of the alloy was not perfectly oriented to the $\langle 100 \rangle$ crystallographic axes.

Thus, the purposes of this work are the following: (1) to study the crystal orientation dependences of the magnetic properties of the single crystal alloys heat-treated in the ridge region of the Fe–Cr–Co system and to clarify whether the FeCo particles are aligned and elongated parallel to the applied field direction, independently of the crystal orientation; (2) to further improve the magnetic properties of Fe–Cr–Co–Mo alloys in developing the $\langle 100 \rangle$ single crystal alloys and also study their crystal orientation dependence of the magnetic properties. These results are discussed in conjunction with their microstructures.

EXPERIMENTAL PROCEDURE

Alloys with the following compositions (in wt %) were chosen for this investigation: Fe–22% Cr–17%Co, Fe–22% Cr–18.5% Co − 3%Mo, and Fe–23% Cr–20% Co-3% Mo alloys. The alloys were melted in an induction furnace from 99.9% electrolytic iron, 99.9% electrolytic chromium, 99.5% cobalt, and 99.8% molybdenum with 1 wt. % titanium as the nitrogen excluding element in air and cast into a cylindrical specimen in a sand mold with an inside diameter of 14 mm. Chemical analysis verified that the final alloy was within 1% of the desired composition. In order to prepare the single crystals, the recrystallization process was used. The preparation of single crystals was described in elsewhere.[5]

The optimum condition of the heat treatment for the ridge single crystals was at first determined by the procedure schematically shown in Fig. 1. After the solution treatment at 1250–1300 °C, the single crystal alloys were aged at 640–730 °C for 10–30 min in a magnetic field of 160 kA/m (2 kOe) and were held at 620 and 600 °C for 1 h each, respectively, followed by the controlled cooling at a rate of 8 °C/h to
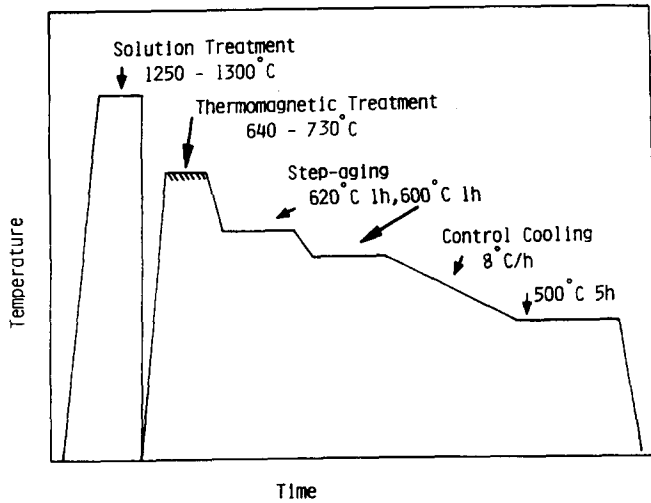
FIG. 1. Schematic diagram of heat treatment.

500 °C and then held at 500 °C for 5 h. This heat treatment is also used to define the temperature of the miscibility gap by monitoring the magnetic properties of the alloys.[16]

Electron microscopy disc specimens were thinned in an automatic jet polisher using an electrolytic solution of 20% perchloric acid and 80% acetic acid. The magnetic properties were measured with an automatic fluxmeter.

RESULTS AND DISCUSSION

The electron micrographs of Fig. 2 show the microstructures of the Fe–22 Cr–17 Co $\langle 100 \rangle$ [Fig. 2 (a) and 2 (b)] and $\langle 110 \rangle$ [Fig. 2(c) and 2(d)] single crystal alloys heat-treated shown in Fig. 1, taken from planes parallel [Fig. 2(a) and 2(c)] and perpendicular [Fig. 2(b), 2(d)] to the direction of the magnetic field. These $\langle 100 \rangle$ and $\langle 110 \rangle$ single crystal alloys were aged at 695 °C for 12 min in the magnetic field along the $\langle 100 \rangle$ and $\langle 110 \rangle$ axes, respectively. The phase with light

FIG. 2. Bright field micrographs of the Fe–22 Cr–17 Co $\langle 100 \rangle$ [(a),(b)] and $\langle 110 \rangle$ [(c),(d)] single crystal alloys aged at 695 °C for 12 min in a magnetic field, followed by the heat treatment shown in Fig. 1. The plane of foils are (a), (c) parallel and (b), (d) perpendicular to the applied field direction ($\uparrow$M).

contrast is the FeCo-rich (α_1) phase, and the phase with dark contrast is the Cr-rich (α_2) phase.[5,11] Referring to Fig. 2, the final product microstructure of $\langle 100 \rangle$ and $\langle 110 \rangle$ single crystal alloys is such that the rod-like ferromagnetic (α_1) phase with a diameter of about 40 nm, a volume fraction of approximately 70%, and a ratio of length to diameter (aspect ratio) of about four is embedded in the (α_2) phase. These microstructural characteristics agree well with reported ones.[17] A similar morphology of the microstructure is observed in the micrograph of the $\langle 111 \rangle$ single crystal alloy. It is important to note that the α_1 particles of the Fe–22 Cr–17 Co single crystal alloys, as shown in Fig. 2(a) and 2(c), are elongated parallel to the direction of the magnetic field, $\langle 100 \rangle$ and $\langle 110 \rangle$, respectively, independent of crystal orientation. In fact, there are practically no differences in the magnetic properties of the Fe–22 Cr–17 Co $\langle 100 \rangle$, $\langle 110 \rangle$, and $\langle 111 \rangle$ single crystal alloys, as shown in Table I.

Although the similar results have been obtained with the Fe–30 Cr–23 Co–1 Si single crystal alloys published in Ref. 5, the Fe–22 Cr–17 Co single crystal alloys yield a high degree of alignment of the α_1 particles induced by thermomagnetic treatment. This higher alignment can be explained by the small difference in the composition of the two phases formed within the ridge region where elastic energy which favors $\langle 100 \rangle$ decompositions is small.[17] Then, the Fe–22 Cr–17 Co single crystal alloys show the excellent squareness of the demagnetization curve defined by Br/Is, as shown in Table I.

Figure 3 shows the electron micrographs of the microstructures of the Fe–23 Cr–20 Co–3 Mo $\langle 100 \rangle$ [Fig. 3(a) and 3(b)], $\langle 110 \rangle$ [Fig. 3(c) and 3(d)], and $\langle 111 \rangle$ [Fig. 3 (e) and 3(f)] single crystal alloys taken from planes parallel [Figs. (a), 3(c), and 3(e)] and perpendicular [Fig. 3(b), 3(d), and 3(f)] to the applied field direction. These single crystals were aged at 670 °C for 12 min in the magnetic field, followed by the heat treatment. The directions of the applied field ($\uparrow M$) of the $\langle 100 \rangle$, $\langle 110 \rangle$, and $\langle 111 \rangle$ single crystal alloys are parallel to $\langle 100 \rangle$, $\langle 110 \rangle$, and $\langle 111 \rangle$ axis, respectively. The microstructure of Fig. 3(a) and 3(b) shows the preferential alignment of
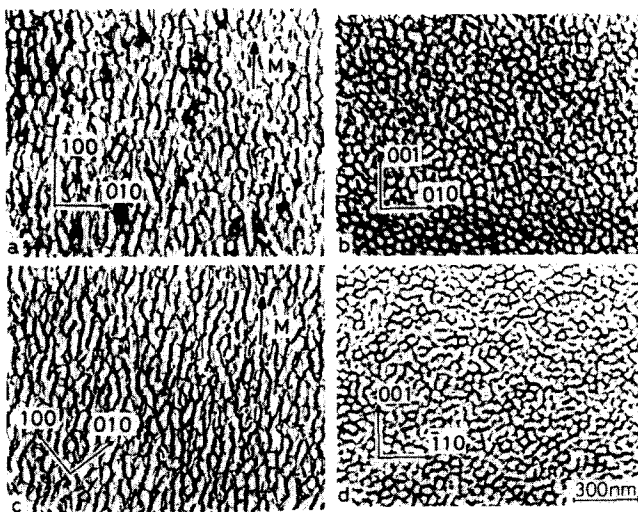
TABLE I. Magnetic properties of the Fe–Cr–Co single crystal alloys without and with 3%Mo.

Specimens	Br (T)	bHc (kA/m)	(BH)max (kJ/m³)	Br/Is (%)
Fe–22 Cr–17 Co				
$\langle 100 \rangle$	1.60	51.7	69.6	97.6
$\langle 110 \rangle$	1.57	50.2	64.0	96.6
$\langle 111 \rangle$	1.57	48.8	61.6	95.7
Fe–22 Cr–18.5 Co–3 Mo				
$\langle 100 \rangle$	1.58	72.8	91.2	98.1
$\langle 110 \rangle$	1.50	54.4	49.6	93.1
$\langle 111 \rangle$	1.36	48.7	36.4	84.4
Fe–23 Cr–20 Co–3 Mo				
$\langle 100 \rangle$	1.48	76.0	88.0	96.2
$\langle 110 \rangle$	1.36	51.2	45.6	89.0
$\langle 111 \rangle$	1.23	45.6	33.6	80.5
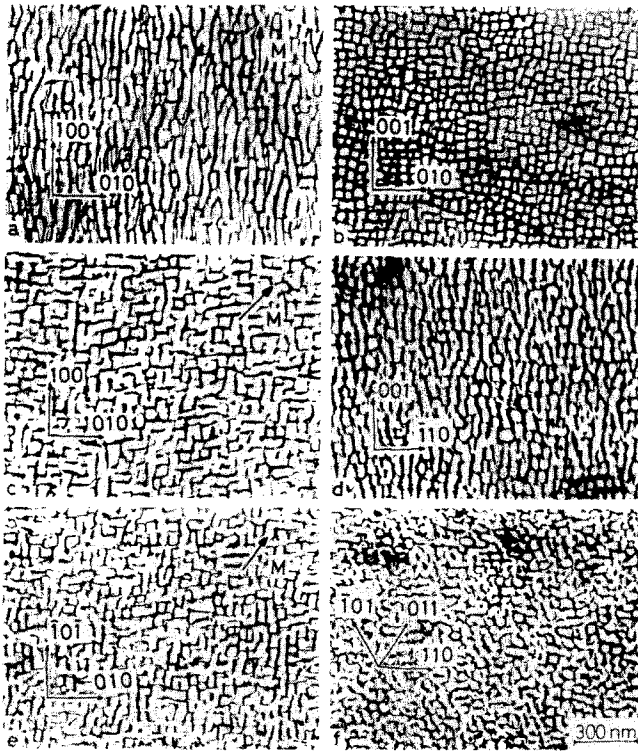
FIG. 3. Bright field micrographs of the Fe–23 Cr–20 Co–3 Mo ⟨100⟩ [(a),(b)], ⟨110⟩ [(c),(d)], and ⟨111⟩ [(e),(f)] single crystal alloys aged at 670 °C for 12 min in a magnetic field, followed by the heat treatment shown in Fig. 1. The plane of foils are (a), (c), (e) parallel and (b), (d), (f) perpendicular to the applied field direction (↑M).

FIG. 4. Effect of angle deviated from a ⟨100⟩ axis on the magnetic properties of the Fe–22 Cr–17 Co, the Fe–22 Cr–18.5 Co–3 Mo, and the Fe–23 Cr–20 Co–3 Mo single crystal alloys. The direction of the applied field is parallel to angle deviated from a ⟨100⟩ axis.

the elongated ferromagnetic α_1 particles parallel to the ⟨100⟩ direction which coincides with the magnetic field direction. The volume fraction of the elongated α_1 particles with the diameter of about 37 nm is approximately 68%. The aspect ratio of the particles is nearly five. On the other hand, Fig. 3(c), which is the electron micrograph taken from the Fe–23 Cr–20 Co–3 Mo ⟨110⟩ single crystal aged in the magnetic field parallel to a ⟨110⟩ axis, shows that the alignment of the ferromagnetic α_1 particles deviates from the direction of the magnetic field shown by arrow (↑M) and the α_1 particles are not exactly aligned along ⟨100⟩ directions and appear to form the interconnecting network along the applied field direction. These morphologies suggest that during decomposition the elastic energy along ⟨100⟩ directions in the Fe–Cr–Co alloys with Mo is higher than the applied magnetostatic energy. A similar morphology of the structure is observed in the micrograph of the Fe–23 Cr–20 Co–3 Mo ⟨111⟩ single crystal alloys shown in Fig. 3(e). The characteristics of those morphologies of the microstructures in Fe–Cr–Co–Mo alloys reflect their magnetic properties.

Figure 4 summarizes the crystal orientation dependence of the magnetic properties of the Fe–23 Cr–20 Co–3 Mo and Fe–22 Cr–18.5 Co–3 Mo single crystal alloys in comparison with those of the Fe–22 Cr–17 Co single crystal alloy. The figure indicates that the ⟨100⟩ single crystal alloys with added Mo have the best magnetic properties and that the greater the deviation from the ⟨100⟩ axis, the poorer are the magnetic properties of the Mo single crystal alloy. From

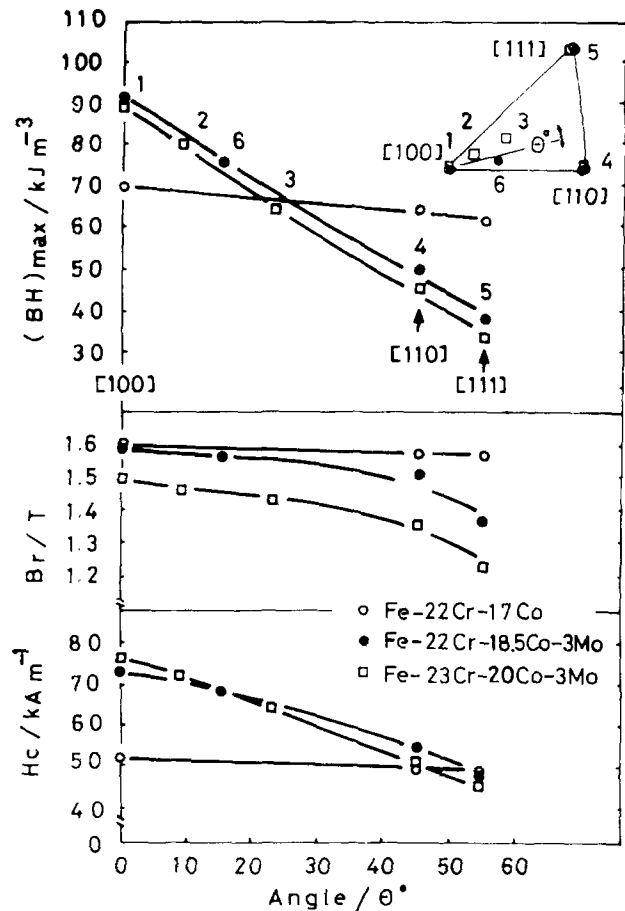the practical point of view in developing the ⟨100⟩ columnar grain structures, it is noteworthy that the Fe–22 Cr–18.5 Cr–3 Mo single crystal alloys yield energy products of (BH)max ⩾ 80 kJ/m^3, as long as the direction of the applied field is within about 12° from a ⟨100⟩ axis. In contrast to the Mo addition alloys, the Fe–22 Cr–17 Co alloy shows almost no orientation dependence of the magnetic properties, which is already stated in Table I.

The best magnetic properties obtained with the Fe–23 Cr–20 Co–3 Mo ⟨100⟩ single crystal are given as Br = 1.48 T (14.8 kG), bHc = 76.0 kA/m (950 Oe), and (BH)max = 88.0 kJ/m^3 (11.0 MGOe). The Fe–22 Cr–18.5 Co–3 Mo ⟨100⟩ single crystal alloy further improved the magnetic properties up to Br = 1.58 T (15.8 kG), bHc = 72.8 kA/m, and (BH)max = 91.2 kJ/m^2 (11.4 MGOe). The corresponding magnetic hysteresis loop of this alloy is shown in Fig. 5 in comparison with that of the Fe–22 Cr–17 Co ⟨100⟩ single crystal alloy. The magnetic properties obtained with Mo addition ⟨100⟩ single crystal alloys are almost comparable to those of a ⟨100⟩ single crystal of an Alnico 8 magnet.[19] It should be mentioned that the optimum procedure of the Fe–22 Cr–18.5 Co–3 Mo single crystal alloys is that the alloys are aged at 675 °C for 12 min in the magnetic field, followed by the heat treatment shown in Fig. 1.
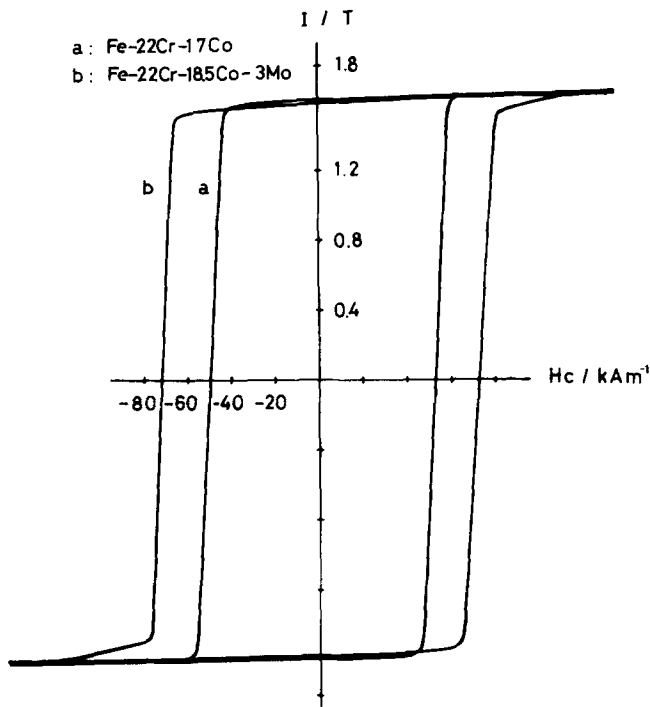
a : Fe-22Cr-17Co
b : Fe-22Cr-18.5Co-3Mo

FIG. 5. Magnetic hysteresis loops of the Fe–22 Cr–17 Co and the Fe–22 Cr–18.5 Co–3 Mo $\langle 100 \rangle$ single crystal alloys.

The summary of the present investigation is as follows. The Fe–22 Cr–17 Co ridge single crystal alloys show the excellent squareness and magnetic properties, independent of crystal orientation. The Fe–Cr–Co–3 Mo single crystal alloys show the clear orientation dependence of their magnetic properties and the more the angle deviated from a $\langle 100 \rangle$ axis

increases, the lesser the magnetic properties are resulted. The best magnetic properties are achieved with the Fe–22 Cr–18.5 Co–3 Mo $\langle 100 \rangle$ single crystal alloy as (BH)max$\simeq$91.2 kJ/m^3 (11.4 MGOe).

[1]H. Kaneko, M. Homma, and K. Nakamura, AIP Conf. Proc. 5, 1088 (1971).
[2]H. Kaneko, M. Homma, K. Nakamura, and M. Miura , IEEE Trans. Magn. MAG-18, 347 (1973).
[3]H. Kaneko, M. Homma, T. Fukunaga, and M. Okada, IEEE Trans. Magn. MAG-11, 1440 (1975).
[4]H. Kaneko, M. Homma, and T. Minowa, IEEE Trans. Magn. MAG-12, 2046 (1976).
[5]H. Kaneko, M. Homma, M. Okada, S. Nakamura, and N. Ikuta, AIP Conf. Proc. 29, 620 (1975).
[6]S. Jin, G. Y. Chin, and B. C. Wonsiewicz, IEEE Trans. Magn. MAG-16, 139 (1980).
[7]S. Jin, and N. V. Gayle, IEEE Trans. Magn. MAG-16, 526 (1980).
[8]M. L. Green, R. C. Sherwood, G. Y. Chin, J. H. Wernick, and J. Bernardini, IEEE Trans. Magn. MAG-16, 1053 (1980).
[9]S. Jin, IEEE Trans. Magn. MAG-15, 1748 (1979).
[10]M. Homma, E. Horikoshi, T. Minowa, and M. Okada, Appl. Phys. Lett. 37, 92 (1980).
[11]M. Okada, G. Thomas, M. Homma, and H. Kaneko, IEEE Trans. Magn. MAG-14, 245 (1978).
[12]Y. Belli, M. Okada, G. Thomas, M. Homma, and H. Kaneko, J. Appl. Phys. 49, 2049 (1978).
[13]S. Mahajan, E. M. Gyorgy, R. C. Sherwood, S. Jin, D. Brasen, S. Nakahara, and M. Eibschutz, Appl. Phys. Lett. 32, 688 (1978).
[14]T. Nishizawa, M. Hasebe, and M. Ko, Acta Met. 27, 817 (1979).
[15]H. Kaneko, M. Homma, K. Nakamura, M. Okada, and G. Thomas, IEEE Trans. Magn. MAG-13, 1325 (1977).
[16]T. Minowa, M. Okada, and M. Homma, IEEE Trans. Magn. MAG-16, 529 (1980).
[17]M. Homma, M. Okada, T. Minowa, and E. Horikoshi, IEEE Trans. Magn. MAG-17, 3473 (1981).
[18]R. Cremer and I. Pfeiffer, Physica B (Utrecht) 80, 164 (1975).
[19]A. I. Luteijn and K. J. De Vos, Philips Res. Rep. 11, 489 (1956).